Celal Bayar University Journal of Science

Tension Field Performance of GFRP Plate Shear Walls

Tuna Ülger[1]* ID

[1] Department of Civil Engineering, Zonguldak Bülent Ecevit University, Zonguldak, Türkiye
* tunaulger@beun.edu.tr
* Orcid: 0000-0002-1758-8299

Abstract

Fiber reinforced polymer (FRP) composites are alternative to the conventional materials for many civil applications because of their prominent properties. The advanced production technology allows standardized structural FRP sections, which plays an important role in progress of the structural engineering. Different fiber types can be rowed in these sections to improve the structural performance of these members. One of the most widely used FRP type is glass FRP (GFRP) in the market for structural use. The plate performance of GFRP materials as a lateral load resisting member within the moment frames was investigated in this study similar to the steel plate shear walls or timber shear walls. Post buckling performance of the GFRP plates including the experimental fracture values and different fiber orientations were studied. The tension field action was considered for the GFRP plates after the post buckling of the moment frame, and it was found that the gain for initial stiffness and story drifts gradually reduced from flexible to rigid moment frames. The least lateral load capacity gain was about 16% when the fiber main direction is oriented 0° angle within the most rigid moment frame. When the fiber orientation aligned within the tension field angle, the load capacity and the initial stiffness was reached to the ultimate values. Finally, analytical load capacity calculations were carried to verify the numerical results of the FRP plate shear walls employing the equivalent truss member approach, then plate thickness and panel aspect ratio effects on were investigated for the GFRP shear walls.

Keywords: FRP plate; FRP fracture; GFRP; lateral stiffness; shear wall; tension field

1. Introduction

The civil structures and construction technologies have been evolved by introducing new techniques, materials, and products. The use of fiber reinforced polymer (FRP) composite materials in rise during recent years. The advances in manufacturing technologies have been playing an important role to the transition from conventional materials to the new advanced materials in structural engineering [1]. Some research efforts are mainly focusing on the use of composite materials with the conventional structures for strengthening, stiffening, retrofitting or restoration applications. The use of fabric FRP materials to enhance the concrete column performance [2–5], and to enhance the flexural and shear capacity of the beams [6–8] were some typical examples in literature and investigated the performance of the structural members considering the effective design parameters such as; fiber orientation, number of composite layers, adhesive types etc. In addition to those interests, new structures and members can be

composed of fully FRP composite members [9–12]. Pedestrian bridges, cooling towers, bridge decks are today`s pioneering composite structures. Pultruded FRP structural shapes are common in the market due to advanced manufacturing technologies. The pultruded FRP plates are commonly designed for the flexural properties like composite deck systems [13–15]. Some research efforts on the other hand are investigated the shear resistance of the steel plates sandwiched between the FRP laminates or fabrics and the load capacity and energy dissipation of FRP bonded steel plates are investigated with various FRP configurations [16–18]. Repair of fatigue cracks by patching FRP on shear plates are studied [19]. Lateral load resistance of the FRP plates by itself can be analogical to the steel plate shear walls (SPSWs) where the slender plate buckles before the full shear resistance, and the tension field actions develops at the post buckling phase of the lateral loadings [20,21]. The studies show that SPSWs can achieve reliable seismic performance with cyclic hysteretic behavior during the post buckling phase [22–27]. The stiffness of the surrounding frame of SPSWs plays an important role in development of the tension

al Bayar University Journal of Science
ume 18, Issue 2, 2022, p 149-160
: 10.18466/cbayarfbe.1015437

T. Ülger

field action [28]. The SPSWs have been effectively utilized in steel buildings with a moment frame to control the story drifts against an earthquake or a wind load which can named a dual lateral load resisting system. Laminated wood plates are another analogical form of a dual system for timber structures [29,30]. It was reported that the cost of the construction can be reduced up to 50% by including the SPSWs in design of the moment frame systems [29]. Considering the prominent properties of composites, FRP plate shear wall system can be preferred instead of steel plate shear wall systems. Even though the initial cost of FRP composites is relatively higher than the cost of steel, the total weight of the structure and the required maintenance cost can be significantly reduced with the proposed FRP shear wall system. Therefore, an adequate lateral performance can be achieved, and the initial cost of FRP can be compensated during the life cycle of the structure [31].

In this study, the flexural fracture of Glass FRP (GFRP) laminates is first determined experimentally to develop an acceptable GFRP fracture mechanism for future analysis. The experimental properties of the tested GFRP laminates were used in numerical modeling and analytical load capacity calculations as well. Then, the lateral performance of three-bare moment frames with various lateral stiffness values are numerically studied with elastic-plastic material properties. The lateral performance of the bare moment frames is enhanced with including infill GFRP plates. The initial stiffness calculations, peak loads and initial fracture mechanisms are presented in the following sections. Finally, the analytical load deflection curves of the GFRP plated moment frames are calculated considering the equivalent truss method. The lateral load-deflection curves are drawn by an iterative method using parallel springs.

2. Experimental Flexural Test of GFRP Specimens

Flexural properties of GFRP strips were determined by using the three-point bending test results and one of the tested specimens at rupture is shown in Figure 1. The average cross section was 9.5 mm x 30.2 mm, and the specimen length was 304.8 mm for the tested five GFRP specimens. In addition to the experimental results, manufacturer`s data sheet was provided for the definition of GFRP materials [32]. The purpose of the experimental tests was the determination of GFRP fracture mechanism and employ similar behavior in latter numerical models. It was calculated for example that the experimentally obtained lengthwise (LW) flexural elastic modulus and fracture stress were about 10% and 88% larger than those provided by the manufacturer`s data sheet, respectively. This discrepancy can be attributed to several factors, but the author believes that this does not the scope of this study. Nevertheless, the lengthwise flexural properties of

GFRP plates were adopted from the experimental three-point bending tests, and they were included in the numerical models.

The experimental bending test results of five specimens were presented in this section. FE element model was developed with the averaged geometrical and mechanical properties to simulate the similar FRP bending and fracture behavior. The experimental results showed that all the specimens had a linear load deflection curve until the load reaches to the fracture load. It was noted that the fracture was initiated at the bottom layers and there was not a visual sign of a compression failure at the top layers as can be seen in Figure 1. The compression failure stress was assumed to be same as the tension failure stress in FE element models. The fracture stress and strain values were included in FE models to start the damage initiation of GFRP plates. Different fracture models can be chosen from ANSYS Mechanical APDL`s [33] material library to simulate the GFRP rapture for the failure simulations; however, the maximum stress fracture model was found in good agreement with the observed fracture behavior, and the results are presented in following sections.
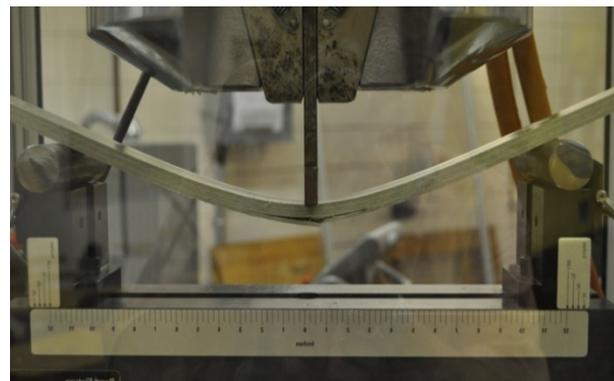
Figure 1. Three-point flexural loading tests of an GFRP strip.

The tipping loads and deflections at the midspan were used to extract elastic modulus and rapture stresses following the procedures given in ASTM D790 [34]. The minimum and maximum elastic modulus can be calculated 18100 MPa and 23500 MPa from the experimental tests, respectively. The average elastic modulus was calculated 21100 MPa for the FE Model simulations. The minimum and maximum peak stresses were calculated 332 MPa and 432 MPa from the experimental tests, respectively. The average of these peak stresses, 389 MPa, was assigned as the maximum failure stress into the GFRP material models. When the maximum stress criterion was satisfied, an assumed stiffness reduction factor, 0.80, was multiplied by the stiffness of the corresponding element; therefore, progressive delamination of GFRP layers was achieved without convergence problems.

Load–deflection curves of the GFRP specimens are presented in Figure 2. The red dashed curve in Figure 2

shows the FE model results in where the averaged experimental properties were assigned. In the FE analysis, the peak load capacity was recorded at 2.64 kN which was about 14% above experimentally obtained average peak load, 2.32 kN. The maximum deflection before the initiation of fracture was 34 mm in the FE analysis which was 13% more than the experimentally obtained average maximum deflection, 30 mm. FE modelling approach and damage propagation were validated with this study, and the measured numerical differences were assumed to be within the acceptable engineering error limits; therefore, GFRP plate shear wall system was modelled using the similar layered material model and mechanical properties, and material fracture model for the rest of the study.
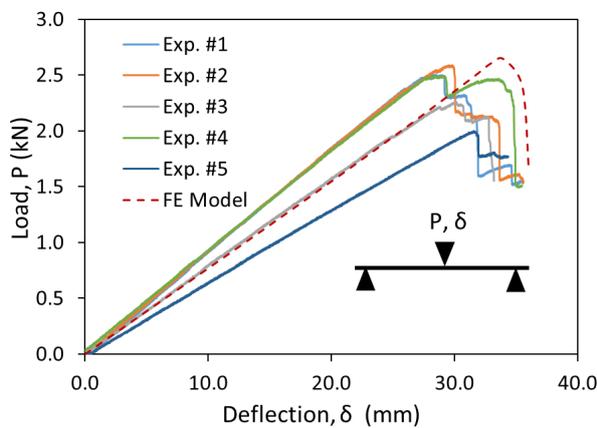
Figure 2. Experimental flexural tests with a FE model simulation.

3. Analytical Formulation of the GFRP Plate Shear Walls

Lateral load capacity of the moment frames which were stiffened with the GFRP plates were approximated using a parallel spring model. The stiffness of the GFRP plate and the steel moment frame were included in capacity calculations before the yield of steel. The stiffness of the moment frame and the deflection at yielding can be easily determined from statics; however, the coupled stiffness of the GFRP plate was not easy to extract from statics for the tension field action. Therefore, the GFRP plate was assumed to be an equivalent truss member where the equivalent truss area was defined by Thorburn *et al.* [28] and given in Equation (3.1). The tension field angle, α, and panel diagonal angle, θ, can be determined using Equations (3.2) and (3.3), respectively, and substituted in Equation (3.1) to find the equivalent truss area, A_{eq}. In these calculations, it was assumed that the columns provide enough rigidity to develop the fully tension field action; therefore, the beam and columns were contributed to the equivalent area of the plate. Also, the shear resistance of the GFRP plate was neglected and only the tension field resistance was accounted in the formulations. Once the

equivalent area of the GFRP plate was determined, the equivalent uniaxial stiffness of the GFRP plate in the tension field was approximated as a truss member. The elastic properties of the GFRP plate were different in lengthwise (LW) and crosswise (CW) directions which required an additional angle to define effective elastic modulus using the combination of orthogonal properties. Simply the effective elastic modulus, E_{F_eq}, was defined as a function of elastic properties and GFRP plate orientation as given in E Equation (3.4). The important part of analytical load capacity calculation was the definition of the failure criteria in the model. Complex failure modes develop in the buckled plate. The first mode is caused by the uniaxial stresses due to tension field and the second is the combination of bending and compression stresses due to plate compression and plate wrinkle in the buckled zones. It should be noted that the GFRP plate had five layers of fibers; therefore, the related stiffness of the section was updated at failure of each fiber layer. The compressive and tensile capacities were assumed equal at those failure limits. Once the extreme fiber reaches the maximum strain limit, the equivalent truss area and related stiffness were recalculated, and the load capacities were calculated by an iterative stiffness updating approach in that spring model. In these calculations, the critical loads were calculated with two-step fracture iterations. In other words, extreme fibers failed two times and equivalent area of the GFRP plate was updated two times for the calculation of analytical load capacities. The numerical results and approximate analytically results are presented in the following result section.

$$A_{eq} = \frac{1/2\ t_F L\ sin^2 2\alpha}{sin\theta\ sin2\theta} \quad \text{(3.1)}$$

$$tan^4\alpha = \frac{t_F L/2A_c + 1}{t_F H/2A_b + 1} \quad \text{(3.2)}$$

$$\theta = tan^{-1}(L/H) \quad \text{(3.3)}$$

$$E_{F\_eq} = \sqrt{(E_{LW}cos\beta)^2 + (E_{CW}sin\beta)^2} \quad \text{(3.4)}$$

4. Numerical Modelling of the Plate Wall Systems

The lateral load capacity of a moment frame with an infill GFRP plates were determined from a single-story moment frame which was subjected to a lateral shear force. The lateral load is applied at the upper beam as a story drift and the total shear forces were recorded at the column bases. The analysis model was sketched in Figure 3, and it shows all the components of the

(a) Moment frame details.   **(b)** Finite Element Model .
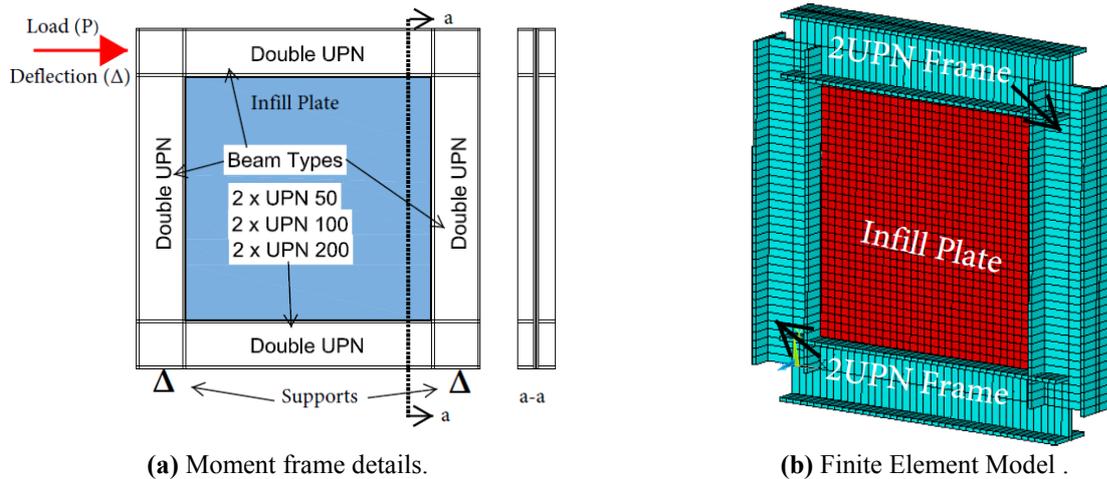
Figure 3. Single story frame and infill plate models.

moment frame. The moment frame was modeled as a steel moment frame and can resist lateral loads without infill plates by the assumed fully rigid joints. The total stiffness of the frame exists due to stiffness of the beams and columns only. Therefore, lateral deflections due to flexibility of the panel zones at the beam-column joints were not included in the total stiffness of the frames. FE model representation of the steel moment frame with infill plate is shown in Figure 3b. The initial stiffness of the moment frames was first determined without the infill GFRP plates to form the base FE model. Then, the GFRP plates were connected to the columns and beams of the surrounding moment frames without allowing the friction losses between the frame and plate. The relative strength and stiffness gain for the base frame with infill GFRP plates were determined in this study.

In the first part of this study, only one panel aspect ratio (plate height divided by width), 1/1 with one slenderness ratio (plate height divided by thickness), 315, is considered. The analytical verification of the FE model results was completed using the equivalent truss beam model and presented with the numerical results. In addition to the GFRP plate shear panels, hypothetical steel plate shear panels were modeled within the same moment frames to compare the performance of steel and GFRP plates. Steel plates were commonly used in the field and research applications as mentioned previous sections; therefore, it is a well-known benchmark candidate for the alternative shear wall systems. The hypothetical steel thickness was determined by equating the bending stiffness of the GFRP to steel plates`. The lateral load resistance of the infilled moment frames was investigated and presented in this section.

In the second part, three different plate thicknesses, 3.2 mm, 6.0 mm and 10 mm, and four different panel aspect ratios,1/2, 1/1, 3/2 and 2/1, were parametrically investigated within the selected moment frames. The GFRP plate width is assumed 1000 mm for all the tested

moment frames while the height of the plates was varied.

4.1 Moment Frames

The test frame was designed to be a steel moment frame with rigid end connections owning lateral stiffness depending on the frame geometry. The frame opening had 1000 mm times 1000 mm a square area, and it was constant for all the cases. In the second part of this study, the panel height was redefined to investigate the different panel aspect ratios for moment frames. The size of columns and beams were identical, and double UPN beams were chosen as the main structural members in numerical analysis with rigid end connections. Two UPN beams were aligned back-to-back to construct the test frames in the FE models. Three different UPN beams from flexible to rigid (UPN50, UPN100 and UPN200) were investigated as the main moment frames to be stiffened with GFRP plates. These beams were modeled using BEAM 188 elements and the strong axis of all the beams were aligned to the loading direction, and the typical frame model is shown in Figure 3b with an infill GFRP shear plate model. The moment frame was loaded at the top beam in horizontal direction by the deflection-controlled method. The total shear load was calculated at the bottom of the plate and load tip deflection was recorded at the loading point. It was assumed that steel follows bi-linear isotropic hardening material model with 235 MPa yield stress and 200000 MPa elastic modulus.

In an experimental test set-up, double UPN beams can be preferable to wrap the perimeter of the plate on both sides by bolting or bonding, so the specimen can be loaded without eccentricity and fixed-fixed boundary condition preserved as presented in this study. In these FE models, the GFRP plate was assumed to be perfectly bonded to the steel frame. Therefore, the stiffness

contribution from the moment frame with and without GFRP plate was similarly accounted.

4.2 GFRP Plates

Pultruded composite sections are layered products where the different number of fiber layers can be rowed within the thickness. The number of layers within the plate can vary and depend on the products and manufacturers; nevertheless, five layers of fibers were counted within the 3.2 mm plate thickness, so the plate was modeled with five layers of fibers and each layer was about 0.63 mm thick. The number of layers were increased as the plate thickness was increased to keep the thickness of each single layer unchanged. GFRP plates were constructed using layered SHELL 181 elements in FE models. Lengthwise properties of GFRP plates were oriented 0°, 45°, and 90° angles in the moment frames and the lengthwise fiber directions for the modeled plates are shown in Figure 4. It may be expected that 0° and 90° angle fiber orientations in a plate show similar results in a square panel; however, tension field angle will yield different failure predictions and load capacities for 0° and 90° angle fiber orientations. The highest load capacity can be expected when 45° angle fiber orientation was aligned with tension field angle; however, it is not practical to locate tension field angle before any theoretical calculations. Even though slightly lesser load capacity can be attained by aligning the lengthwise fibers to the panel diagonal, it is more practical to apply 45° angle in real life structures. Nevertheless, the expected fracture mechanism for three different panels with three fiber orientations was addressed in the first part of the study as shown in Figure 4, and in the second part of the study only 45° angle fiber orientation was investigated with different panel aspect ratios.
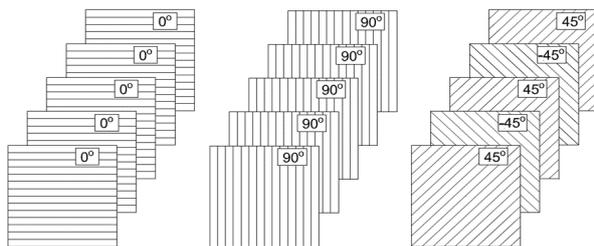
Figure 4. Fiber orientation angles within the tested GFRP plates.

The geometric nonlinearity is considered in FE models by providing an initial out-of-plane distortion to the GFRP plates. Most of the structural elements have some sort of geometrical imperfections that cause the secondary stresses. In those fabricated products, possible out-of-straightness exists before and after the installation of the GFRP plates. Different methods can be used to include the initial imperfections. The first

buckled mode shape of Eigen Buckling analysis was assigned to the plates. It was noted that some varied distortional ratios, 1/2000 and 1/500, did not show significant load capacity changes but yield different post buckling convergence issues for the considered thin GFRP plates. The assumed distortion was the 1/1000 of the plate heights, which conclude a unit distortion in the model for the square infill plates.

4.3 Steel Plates

Steel plate shear walls (SPSW) are commonly used in structural applications. In this study, SPSW is considered as a benchmark method in research of GFRP plate shear walls. The steel plate was modeled homogenous non-layered shell element. The mechanical properties were assumed identical to the moment frame where the plate has 235 MPa yield stress and 200000 MPa elastic modulus with elastic perfectly plastic bilinear material model. The hypothetical thickness of the steel plate was calculated 1.501 mm by equating the bending stiffness of the plates. Initial imperfections of the steel plates were included in FE analysis by employing the deformed shape of first Eigen Buckled mode; therefore, tension field action developed within the steel plates.

4.4 Mesh Study of the FE Model

In the developed FE model, meshing is an important step for the plate analysis where the buckling occurs, the fracture propagates in the tension and compression zones. Therefore, different element sizes were studied for the GFRP plates within the moment frames. The plate mesh topology was followed by the columns and beams. The results showed that the difference in the load-deflection results were in the decimal places for relatively fine meshes; 50 mm, 25 mm, and 10 mm element sizes. However, it can be said that the convergence of these element sizes in FE model slightly differs due to progressive fracture of the GFRP plates. In this study, 25 mm element size is chosen for analysis of all the FE models. Therefore, the meshed GFRP plates were represented at least with 1600 elements in 1000 mm x 1000 mm plate areas.

5. Test Results
5.1 Analytical Results of the Moment Frames

Approximate load capacities of the GFRP plate shear wall systems were obtained using the equivalent truss member method. The FE model results are only presented for 0° and 45° angle fiber oriented GFRP plates in Figure 5 and 6, respectively. Steel moment frames yielded before the rupture initiation of the GFRP plates. Initial lateral stiffnesses of the numerical models were in good agreement with total spring stiffness that was used in the analytical calculations when the and the
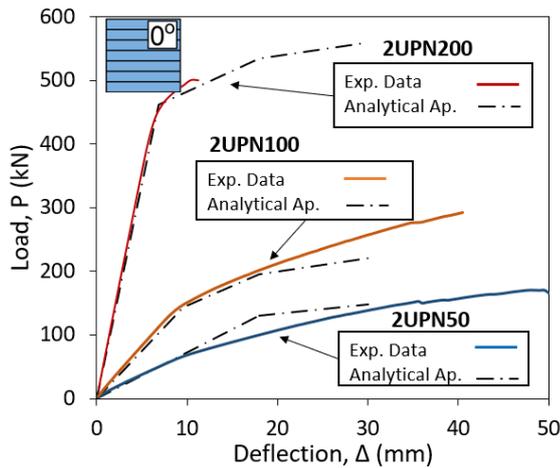
Figure 5. Load – deflection curve of the moment frames for 0° fiber orientation angle.
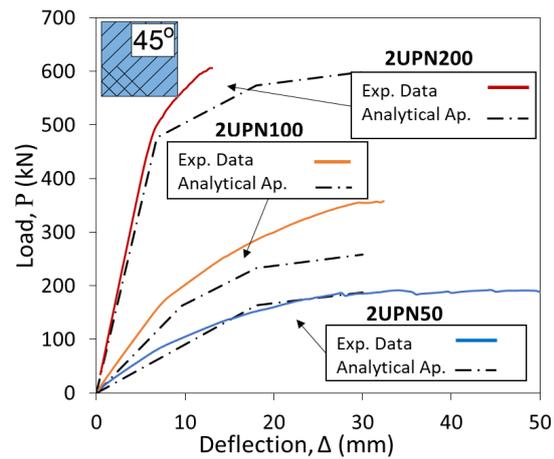
Figure 6. Load – deflection curve of the moment frames for 45° fiber orientation angle.

Table 1. Initial stiffness ratio of numerical and analytical calculations.

Moment Frames	GFRP Plate Orientation					
	0°	90°	45°	0°	90°	45°
	$E_{i\ numerical}$ / $E_{i\ analytical}$			$P_{u\ numerical}$ / $P_{u\ analytical}$		
2UPN 50	1.01	1.10	1.23	0.87	0.80	0.90
2UPN 100	1.06	1.09	1.27	1.01	1.01	1.07
2UPN 200	1.06	1.06	1.12	0.81	0.85	0.75

Ei: Initial Stiffness; Pu: Ultimate load capacity

lengthwise fiber oriented 0° angle as shown in Figure 5. Slight difference can be seen for the initial stiffness of the tested frames when the fiber was oriented 45° angle, latter can be seen in Figure 6. In Figure 5 and 6, after the steel frame yields, the lateral stiffness of that frame was neglected, and equivalent truss member stiffness resist the lateral load until the extreme fiber layers reached to critical failure stress. It was calculated that the moment frames reached about 21.8 mm lateral deflection until the first fiber rupture. The effective height of the section was recalculated after the first rupture of GFRP layers from top and bottom of the section. The GFRP section`s loss was accounted by updating the effective elastic modulus and effective area of the GFRP plates for the second iteration. The second iteration was completed when the next unfailed extreme fiber reached its critical stress state. In other words, the residual stress capacity of the internal fibers was recalculated by an iterative approach until the critical stress was exceeded. The further iterations can be completed to obtain stiffness losses until the rapture of the last internal fiber, but the calculations were not considered after the second iteration.

The numerical difference between the initial stiffness and peak loads of the numerical and analytical calculations are presented as the ratio of the results in Table 1, respectively. The maximum initial stiffness ratio was 1.27 for the 2UPN 100 frame and the average ratio is about 1.21 for all three moment frames when the

plate oriented at 45° angle. When the fiber was oriented 0° and 90° angles, the average initial stiffness ratio is 1.07 for these moment frames as given in Table 1. Peak load ratios between the numerical and analytical calculations were presented in Table 1. The numerical results for the 2UPN 200 frame did not converge at the post buckling load capacities; therefore, the last step solutions were given as their peak load ratios in Table 1. The maximum peak load difference was calculated 0.75 for the non-converged solution of 2UPN 200 frame when the plate oriented at 45° angle. The average ratio can be calculated 0.89 for all the moment frames considering all the fiber orientations. This result showed that the analytically predicted peak loads were generally higher than the peak loads of the numerical results. Another analytical approach can be the inclusion of load drops at each fiber rupture. Once the fiber ruptures, the force needs to be balanced at the same deflection with equivalent adjusted stiffness and equivalent area which causes the load drop until the new stress equilibrium satisfied. However, this load drops were not included in the current analytical calculations, and the obtained results were found to be adequate to validate the numerical model results.

It should be noted that the error in these approximations can be calculated by assuming different failure definitions; therefore, initial failure criterion played an important role in these capacity predictions.

Table 2. Ultimate load capacity and load capacity increase of the moment frames.

Test Frames	Plate Thickness (mm)					
	--	1.501	3.175		3.175	
	P_u_MF (kN)	P_u_SP (kN)	P_u_FP_0° (kN)	P_u_SP - P_u_FP_0°	P_u_FP_45° (kN)	P_u_SP - P_u_FP_45°
2UPN 50	20.6	137	147	6.80%	187	26.74%
2UPN 100	91.3	259	282	8.16%	354	26.84%
2UPN 200	416	612	505	-21.19%	612	0.00%

MF: Moment frame, SP: Steel Plate Shear Wall, FP: GFRP Plate Shear Wall, Pu: Ultimate load capacity

Table 3. Initial stiffness and deflections of the moment frames at their initial yield points.

Moment Frames	Steel Plate		0° FRP Plate		45° FRP Plate	
	E_i (N/mm) [%]	Δ_i (mm) [%]	E_i (N/mm) [%]	Δ_i (mm) [%]	E_i (N/mm) [%]	Δ_i (mm) [%]
2UPN 50	42150 [4053]	3.5 [82]	7240 [613]	9.6 [50]	11167 [1000]	8.0 [58]
2UPN 100	64207 [638]	5.0 [52]	16689 [92]	8.0 [23]	22677 [161]	8.0 [23]
2UPN 200	138950 [123]	2.5 [60]	72090 [16]	6.1 [16]	79000 [27]	6.1 [16]

E_i: Initial stiffness, Δ_i: Lateral deflection

5.2 Numerical Results of the Square GFRP Plates

Lateral load resistance of steel moment frames was analyzed without GFRP infill plates, and these were called as the base frame performances. The base frames with double UPN (2UPN) 50, 100 and 200 beams reached about 19.2 mm, 10.4 mm, and 6.5 mm deflections at their 20 kN, 91 kN, and 416 kN peak lateral loads, respectively. These critical peak loads for the steel plates and initial rupture of the GFRP plates were given at peak loading Table 2. The 90° angle fiber orientation was omitted in Table 2 because 0° and 90° fiber angles produced similar load capacities.

The maximum load capacity gain was obtained when GFRP plate positioned with 45° angle fiber orientation. The stiffer moment frame reduced the relative load capacity increment for steel and GFRP plates. Only the load capacity of GFRP plate stayed below the steel plate`s when the GFRP plate was oriented at 0° or 90° fiber angles in the most rigid steel frame. Therefore, the proper alignment of the lengthwise fiber angle can result more load capacity increment for GFRP plate than steel plate shear wall systems. On the other hand, elastic stiffness and post buckling stiffness of the steel plate shear walls were significantly superior to the GFRP plates for the considered moment frames. The increment for the initial stiffness and lateral deflections at failure over the base moment frames can be seen in Table 3. These deflections can be read as the story drift of a single-story frame and the reduction was a gain or vice versa for the recorded deflections at their failure points on the load-deflection curves. This showed that the hypothetical steel and GFRP plates can reduce the story drifts as low as 52% and 16%, respectively. These story drifts can be reduced more when the flexible moment frames were needed to be stiffened. Fiber orientation was another effective parameter for the reduction of the story drifts. The graphical representation of the

considered moment frames with steel and GFRP plates were plotted in Figure 7 to 9. A small difference was observed between the load deflection curves of 0° and 90° angle fiber oriented GFRP plates, and this difference became negligible when the lateral stiffness of the steel frame was increased. Theoretically, this difference can be attributed to the difference between the panel diagonal angle and tension field angle. Another difference was observed in the initiation and propagation of the GFRP fiber ruptures during the post yielding of the steel frames. The yield deflections were improved with flexible steel frame as can be seen in Figure 7, but this improvement gradually reduces as the lateral stiffness of the steel frame was increased as shown in Figure 9.

When the fiber angle was oriented parallel to the diagonal, 45°, the increase in lateral stiffness and load capacity were obtained. Hypothetical steel plates were provided around four times stiffer response than the GFRP plates in linear loading phase, and almost stable load capacity change observed during the post buckling phase. Toughness of the moment frames was defined in Table 4 with assumed deflection limits when the first rupture of GFRP was initiated; therefore, yielding of steel and progressive rupture of GFRP were excluded in these calculations. The total toughness of the GFRP plate shear walls with 0° fiber orientation was 32.4% below the toughness of steel plate. The fiber orientation at 45° angle for the GFRP plates improved the total toughness. The difference between the steel and GFRP plate shear walls was almost negligible, less than 1.0%, for 2UPN50 and 2UPN100 frames. However, the GFRP plate within the stiffer frame 2UPN200 showed 19.4% less fracture toughness than the steel plate shear wall system. Therefore, the stiffer moment frame requires thicker GFRP plate to reach the similar toughness of benchmark steel plate shear wall systems.

Table 4. Fracture toughness of the moment frames with infill plates

| | | **Plate Thickness (mm)** | | | | |
| | | -- | 1.501 | 3.175 | | 3.175 |
Test Frames	**Deflection Cut-off, Δ_c, (mm)**	**T_SP (kNmm)**	**T_FP_0° (kNmm)**	**T_SP - T_FP_0°**	**T_FP_45° (kNmm)**	**T_SP - T_FP_45°**
2UPN 50	28	3274	2244	-45.9%	3254	-0.62%
2UPN 100	30	6808	5143	-32.4%	6825	0.25%
2UPN 200	13	6161	4570	-34.8%	5160	-19.40%

T: Fracture toughness, Δc: deflection state for toughness calculation, SP: Steel Plate Shear Wall, FP: GFRP Plate Shear Wall
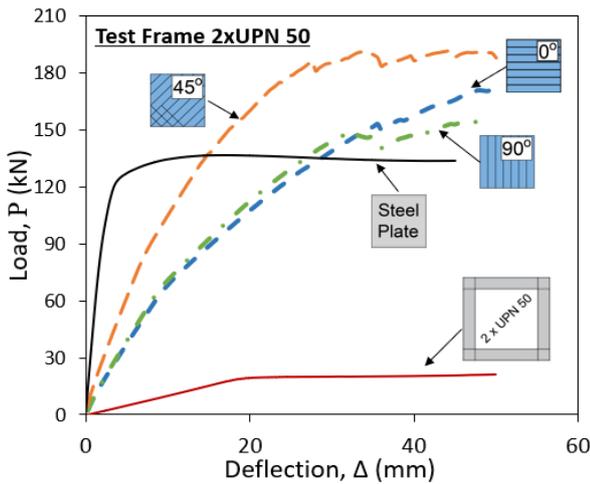
Figure 7. The load-deflection curve of 2UPN 50 moment frame with/without shear plates.
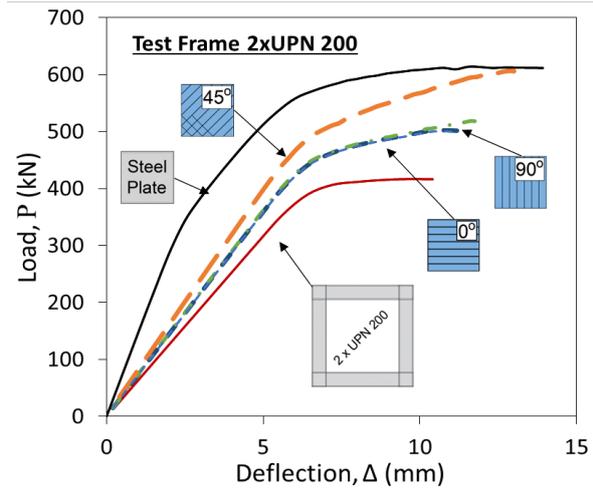
Figure 9. The load-deflection curve of 2UPN 200 moment frame with/without shear plates.

The average of the experimentally obtained uniaxial failure strain was also plotted with a black dotted line in those figures to provide an approximate uniaxial failure strain.

The most straining effect can be seen in 2UPN 50 beams with the plate thickness of 3.2 mm as shown in Figure 10. Two ends of the tension field diagonal were strained the most in the 2UPN50 beam, and this straining effect was smaller around the middle of the tension field diagonal, which was about the center of the GFRP plate. Therefore, it was concluded that the initiation of the failure for the considered GFRP plate shear walls were the end connections of the moment frames. Compression and tension field diagonals cross each other at the center, and both shows an identical straining effect at the same location. That location is about the maximum straining location for the compression field diagonal and the strains become relatively negligible at the end of the compression field diagonal.

Figure 8. The load-deflection curve of 2UPN 100 moment frame with/without shear plates.

The averaged elastic equivalent strains along the tension and compression fields were recorded at the GFRP plates` peak load capacities. The solid and dashed lines represent the tension and compression field strains respectively in Figure 10 to 12. Strain readings were extracted only for the 45° GFRP plate orientation in this study.

In a cyclic loading of a GFRP shear wall system, the four corner regions of the plate will be subjected to the more intensified stresses and needs to be protected for thinner plates to eliminate immature failures. As the plate thickness or the lateral stiffness of the steel frame
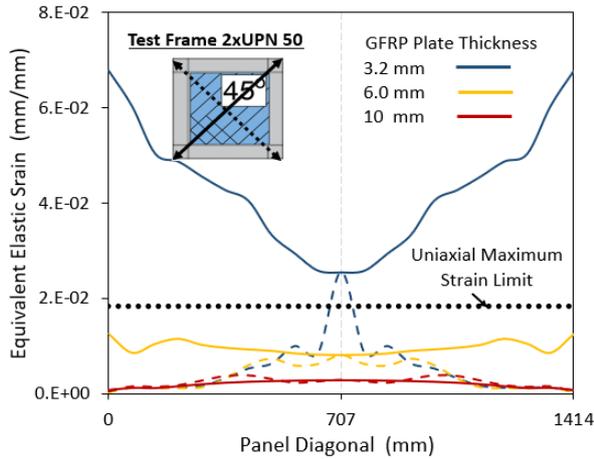
Figure 10. Tension (solid lines) and compression (dashed lines) field equivalent strains for 2UPN 50 frame.
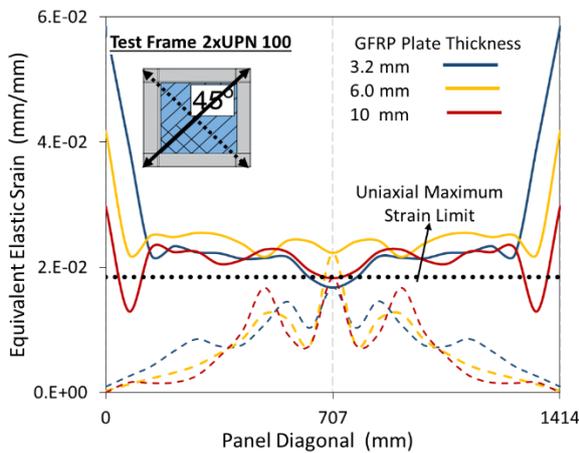
Figure 11. Tension (solid lines) and compression (dashed lines) field equivalent strains for 2UPN 100 frame.
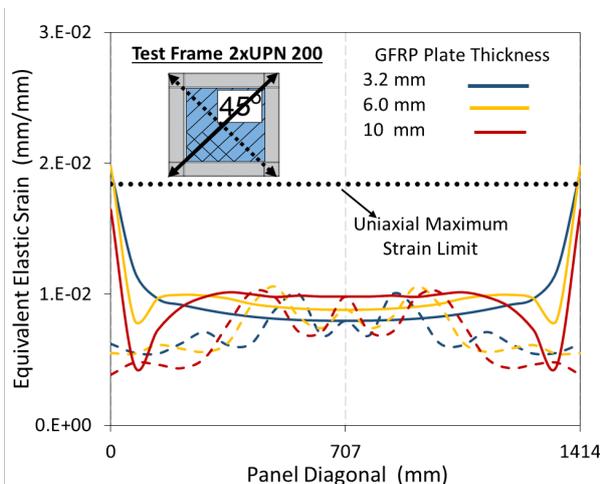
Figure 12. Tension (solid lines) and compression (dashed lines) field equivalent strains for 2UPN 200 frame.

increases, the straining action on the diagonals tends to reduce gradually as can be seen in Figure 11 and 12. The increased stiffness of the steel frame results more unified straining action on the GFRP plate up to their peak loads. It should be noted that the convergence of the load capacities may slightly alter the strain values at the peak loads; however, the equivalent strains with different steel frames and plate thicknesses provide the possible failure pattern of the GFRP plate. Therefore, the tension field action can be developed with relatively thicker plates and the straining action become more uniform along the plate diagonals.

The detailed study of the infill plated steel moment frames using either steel or GFRP plates showed that the tension field action was developed with the thin plates. Flexible moment frames were benefited more from the use of shear plates even though the full tension field action cannot be developed within the flexible frames [28]. The reduced story drifts were delayed the yield of the moment frames, and the yield load capacity of those frames were also increased using the shear plates. However, the yield point of the rigid moment frames almost was not affected from the tension field action as shown in Figure 9.

5.3 Results of Different GFRP Panel Aspect Ratios

The different plate slenderness and panel aspect ratios of the GFRP plate shear wall systems were investigated, and their normalized peak load capacities are given in this section. Each GFRP plate shear wall frame`s peak loads were normalized using its corresponding base frame`s load capacity to be able present the relative load capacity ratios. In this section four different panel aspect ratios, panel height divided by panel width, were considered with three different GFRP plate thickness. These thicknesses created different plate slenderness within the considered moment frames. In this study, 1000 mm wide panel width was kept unchanged and panel height was varied to have the panel aspect ratio of 1/2, 1/1, 3/2 and 2/1. Three different thicknesses were selected considering the commercial availability of the GFRP plates and they were placed to be oriented at 45° angle within the moment frames. This angle was not guaranteed the best performance for some of the panel aspect ratios due to variation of the tension filed angle according to the panel aspect ratios; however, 45° fiber orientation can be assumed one of the most practical approaches in the field applications. In other words, the lateral resistance of the GFRP plates can be increased some amount from the presented load capacity ratios when the lengthwise fiber angle was aligned with the theoretical tension field angles. Nevertheless, the presented results are still valid for the assumed GFRP plate orientation and that minimum and maximum angle difference is 0° and 7° for the 1/2 and 2/1 panel aspect ratios, respectively. The results were presented in Figure 13 to 15 with custom markers, and these markers

al Bayar University Journal of Science
ume 18, Issue 2, 2022, p 149-160
: 10.18466/cbayarfbe.1015437

T. Ülger

represent the panels in scale so the reader can easily follow the change in load capacity ratios for different panel aspect ratios. The customized black lines in the same figures represent the same GFRP plate thickness for different set of panel aspect ratios.

Typical two general results were concluded from the parametric results of the GFRP plate shear wall system. The first one is the increased plate slenderness reduces the load ratios, and the second is the increased plate thickness increases the load capacity ratios in all moment frames. Another common result for all the moment frames was that the normalized load capacity ratio was the highest for the largest panel aspect ratio within the same thickness category, and that normalized capacity ratios gradually decreases as the panel aspect ratio decreases. Finally, it can be concluded from the trend of these plots that the panel aspect ratio larger than 2/1 will not yield significant load capacity increase for the considered moment frames.
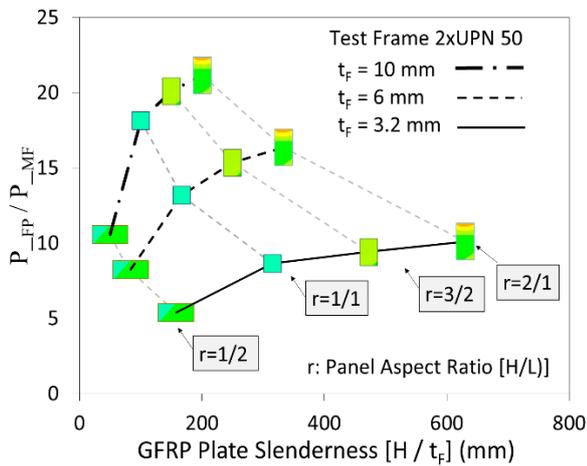
Figure 13. Plate slenderness effect with different panel sizes for 2UPN 50 moment frame
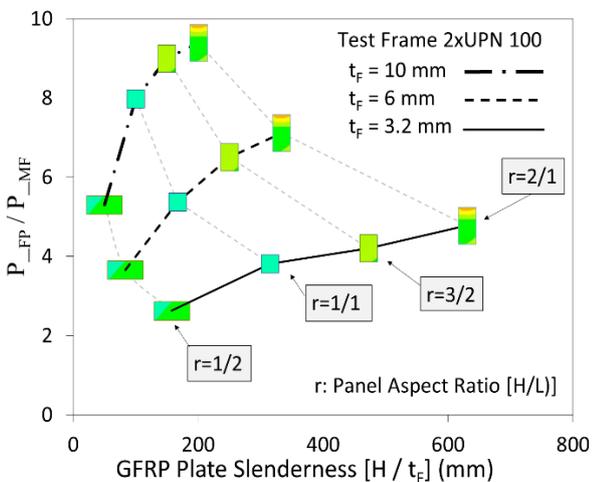
Figure 14. Plate slenderness effect with different panel sizes for 2UPN 100 moment frame
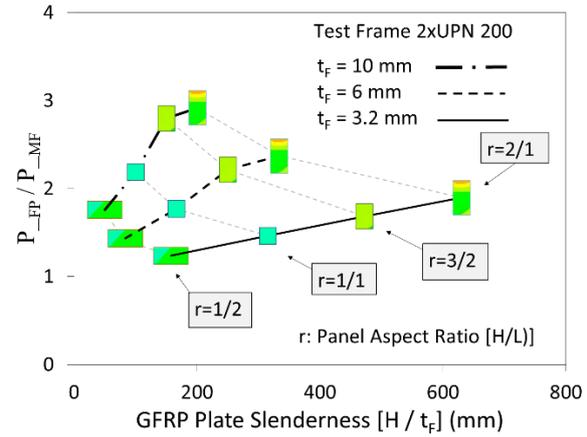
Figure 15. Plate slenderness effect with different panel sizes for 2UPN 200 moment frame

The higher load capacity ratios were obtained while stiffening the more flexible moment frames as described earlier for the square panel beams. The moment frame with 2UPN 50 beams can reach the load capacity ratio of 5 to 21 as the plate thickness ranges from 3.2 mm to 10 mm, respectively. The change in the capacity of that frame is shown in Figure 13. These load capacity ratios for the same thicknesses get decreased to the range of 2.6 and 9.2 when the 2UPN 100 beam was considered as the steel moment frame as shown in Figure 14. Finally, the load capacity ratios for the same thicknesses become narrowed down to 1.2 to 2.9 for the relatively rigid frame, 2UPN 200 beams in Figure 15, respectively.

5. Conclusions

The study aimed to enhance the lateral load capacity of a moment frame with an infill GFRP plates taking the advantage of the composite material properties. Commercially available thin GFRP plates were selected in this study. These plates can buckle before the critical shear load capacities so the full shear resistance cannot develop within the plate. Therefore, tension field action can develop after the plate buckling. The numerical models were first developed and then verified to study the performance of square GFRP plates in a moment frame. The material properties and failure criterion for the GFRP specimens was extracted from the experimental results of the three-point bending tests. An analytical method using an equivalent truss member stiffness was presented to approximate and verify the lateral load capacities of a single-story moment frames. As a result of the analytical formulation, not only the peak load capacities but also the load deflection history of the moment frames was presented in this paper. Hypotetical steel plate was defined instead of GFRP plates within the moment frames to compare the lateral response of two different materials. Finally, different plate thicknesses with different panel aspect ratios were

parametrically studied with the verified numerical models, and all related findings were listed below:

• Tension field action can develop in GFRP plates until the initial rupture. After that rupture, the degradation of fibers reduces the load capacities.

• The effectiveness of the GFRP plate is highly dependent on the base moment frame`s lateral stiffness. The flexible moment frames produce the highest load capacity and initial stiffness increase or vice versa. The least load capacity and initial stiffness increments are about 21% and 16%, respectively, for the most rigid moment frame.

• The resistance of the tension field depends on the lengthwise and crosswise properties of the GFRP plates. The most gain can be attained when the GFRP plate`s lengthwise direction is aligned with the tension field angle. The numerical study showed that the 45° angle fiber orientation showed the ultimate gain in this study.

However, it was found that even for the square plates, tension field angle slightly differs than 45°; therefore, 0° and 90° angle fiber orientations showed slight difference in their initial stiffness and peak load capacities.

• The hypothetical steel plate showed the most initial stiffness increase by 123% in this study. Following the steel plate yielding, there is flat post buckling zone obtained without rupture since the steel is modeled as elastic - perfectly plastic material. It can be concluded from the load deflection curves that the elastic energy stored in the steel plates was higher than the GFRP plates`. On the other hand, GFRP plate still weighs lighter than the hypothetical steel plate for the considered GFRP plate thicknesses.

• The numerical studies showed that the peak load capacities of the GFRP plates were either above or same as the steel plate`s for the square moment frames. However, the initial stiffness of the steel plate was found 4 times more than the GFRP plate`s.

• The approximated analysis provided an iterative analytical solution including the fiber failures. These formulations can be used to verify the numerical results.

• Considering the same plate thicknesses within the different panel aspect ratios, the largest panel aspect ratio, 2, showed the highest normalized load capacity increase than that of the others.

• When the panel aspect ratio of a frame was larger than 2, that panel was provided significant load capacity increase for the considered moment frames.

In summary, while the GFRP plates can be utilized to enhance the load capacity and reduce the relative story drifts, they can be as effective as the steel plates. The mechanical properties and light weight of the composite panels can be an alternative for steel or wood plate shear wall applications. This results courage the researchers to perform further experimental test to obtain static and cyclic performances of the GFRP plate shear walls.

Author's Contributions

Tuna Ülger: Drafted and wrote the manuscript, performed, and interpreted the whole experiments and analysis.

Ethics

There are no ethical issues after the publication of this manuscript.

References

[1]. Frketic, J, Dickens, T, Ramakrishnan, S. 2017. Automated manufacturing and processing of fiber-reinforced polymer (FRP) composites: an additive review of contemporary and modern techniques for advanced materials manufacturing. *Additive Manufacturing*; 14: 69–86.

[2]. Green, MF, Bisby, LA, Fam, AZ, Kodur, VK. 2006. FRP confined concrete columns: Behaviour under extreme conditions. *Cem. Concr. Compos.*; 28(10): 928–937

[3]. Arghya, D, Bhattacharyya, SK. 2010. Investigation into the effect of bonding on FRP-wrapped cylindrical concrete columns. *J. Compos. Constr.*; 14(6): 706–719.

[4]. Pham, TM, Hadi, MNS, Jim, Y. 2015. Optimized FRP wrapping schemes for circular concrete columns under axial compression. *J. Compos. Constr.;* 19(6): 4015015.

[5]. Wang, Z, Wang, D, Smith, ST, Lu, D. 2012. Experimental testing and analytical modeling of CFRP-confined large circular RC columns subjected to cyclic axial compression. *Eng. Struct.*; 40: 64–74.

[6]. Saadatmanesh, H, Malek, AM. 1998. Design guidelines for flexural strengthening of RC beams with FRP plates. *J. Compos. Constr.*; 2(4): 158–164.

[7]. Elsanadedy, HM, Almusallam, TH, Alsayed, SH, Al-Salloum, YA. 2013. Flexural strengthening of RC beams using textile reinforced mortar – experimental and numerical study. *Compos. Struct.;* 97: 40–55.

[8]. Rasheed, HA, Zaki, MA, Foerster, AS. 2022. Efficient bidirectional U-wrap system to anchor CFRP sheets bonded to reinforced concrete T-girders. *Structures*; 38: 226–236

[9]. Van Den Einde, L, Zhao, L, Seible, F. 2003. Use of FRP composites in civil structural applications. *Construction and Building Materials*; 17(6): 389–403.

[10]. Sonnenschein, R, Gajdosova, K, Holly, I. 2016. FRP composites and their using in the construction of bridges. *Procedia Engineering*; 161: 477–482.

[11]. Alshurafa, S, Alhayek, H, Polyzois, D. 2021. Static characteristics of multicells jointed FRP tower with mass on its top. *Mechanics of Advanced Materials and Structures*; 28(3): 229–236.

[12]. Wang, Y, Chen, G, Wan, B, Han, B, Ran, J. 2021. Axial compressive behavior and confinement mechanism of circular FRP-steel tubed concrete stub columns. *Composite Structures*; 256: 113082.

al Bayar University Journal of Science
ume 18, Issue 2, 2022, p 149-160
: 10.18466/cbayarfbe.1015437

T. Ülger

[13]. Salim, HA, Davalos, JE, Qiao, P, Kiger, SA. 1997. Analysis and design of fiber reinforced plastic composite deck-and-stringer bridges. *Composite Structures*; 38(1): 295–307.

[14]. Cheng, L, Karbhari, VM. 2006. New bridge systems using FRP composites and concrete: a state-of-the-art review. *Progress in Structural Engineering and Materials*; 8(4): 143–154.

[15]. Oludare, O, Elias, T. 2019. In-plane shear characterization of composite GFRP-foam sandwich panels. *Journal of Composites for Construction*; 23(5): 4019034.

[16]. Nateghi-Alahi, F, Khazaei-Poul, M. 2012. Experimental study of steel plate shear walls with infill plates strengthened by GFRP laminates. *Journal of Constructional Steel Research*; 78: 159–172.

[17]. Edalati, SA, Yadollahi, Y, Pakar, I, Bayat, M. 2015. On the effect of GFRP fibers on retrofitting steel shear walls with low yield stress. *Earthquakes and Structures*; 8: 1453–1461.

[18]. Petkune, N, Donchev, T, Hadavinia, H, Limbachiya, M, Wertheim, D. 2016. Performance of pristine and retrofitted hybrid steel/fibre reinforced polymer composite shear walls. *Construction and Building Materials*; 117: 198–208.

[19]. Bach, D, Akhrawat, L. 2020. Optimization of fiber-reinforced polymer patches for repairing fatigue cracks in steel plates using a genetic algorithm. *Journal of Composites for Construction*; 24(2): 4020006.

[20]. Ronny, P, Michel, B. 2009. Finite-element investigation and design recommendations for perforated steel plate shear walls. *Journal of Structural Engineering*; 135(11): 1367–1376.

[21]. Azarafrooz, A, Shekastehband, B. 2020. Behavior of fully-connected and partially-connected multi-story steel plate shear wall structures. *Structural Engineering and Mechanics*; 76(3): 311–324.

[22]. Mirmura, H, Akiyana, H. 1977. Load-deflection relationship on earthquake-resistant steel shear walls developed diagonal tension field. *Transactions of the Architectural Institute of Japan*; 260: 109–114.

[23]. Vincent, C, Mohamed, E, Ruobo, C. 1993. Experimental study of thin steel-plate shear walls under cyclic load . *Journal of Structural Engineering*; 119(2): 573–587.

[24]. Ramla, Q, Michel, B. 2019. Behavior of steel plate shear walls subjected to repeated synthetic ground motions. *Journal of Structural Engineering*; 145(4): 4019008.

[25]. Deng, E-F, Zong, L, Wang, H-P, Shi, F-W, Ding, Y. 2020. High efficiency analysis model for corrugated steel plate shear walls in modular steel construction. *Thin-Walled Structures*; 156: 106963.

[26]. Damghani, M, Wallis, C, Bakunowicz, J, Murphy, A. 2021. Using laminate hybridisation (CFRP-GFRP) and shaped CFRP plies to increase plate post-buckling strain to failure under shear loading. *Thin-Walled Structures*; 162: 107543.

[27]. Lu, J, Zhang, H, Yu, S. 2021. Study on seismic behaviors of self-centering steel plate shear walls with slits. *Journal of Constructional Steel Research*; 185: 106878.

[28]. Thorburn, LJ, Montgomery, CJ, Kulak, GL. Analysis of steel plate shear walls, Edmonton, Alberta, 1983.

[29]. Dolan, JD, Foschi, RO. 1991. Structural analysis model for static loads on timber shear walls. *Journal of Structural Engineering*; 117(3): 851–861.

[30]. Bryan, F, Andre, F. 2001. Cyclic analysis of wood shear walls. *Journal of Structural Engineering*; 127(4): 433–441.

[31]. Ilg, P, Hoehne, C, Guenther, E. 2016. High-performance materials in infrastructure: a review of applied life cycle costing and its drivers – the case of fiber-reinforced composites. *Journal of Cleaner Production*; 112: 926–945.

[32]. Bedford Reinforced Plastics. Bedford Structural Shapes. https://bedfordreinforced.com/products/proseries/proforms/ (accessed at 13.10.2021).

[33]. ANSYS Academic Research Mechanical, Release 15. Mechanical APDL Material Reference.

[34]. ASTM D790. 2015. Standard Test Method for Flexural Properties of Unreinforced and Reinforced Plastics and Electrical Insulating Materials. West Conshohocken, PA, USA: ASTM International.